The Elastic Properties of Single Crystals with Microstructure and Applications to Diffusion Induced Segregation

T. Blesgen[*,1]

[1] Max-Planck-Institute for Mathematics in the Sciences, Inselstraße 22-26, 04103 Leipzig, Germany

Received 2008-04-22
Published online

Key words Structure gradients, general theory of continuum mechanics of solids, microstructure
PACS 2.60.Cb, 46.05+b, 61.50Ks, 61.72.-y

In this article a general theory for elastically stressed solids in the presence of microstructure is presented and an explicit formula for the resulting non-linear stored mechanical energy is obtained. The optimal microstructure under applied stress is characterised and the optimal laminates are identified in 2D. The analysis is based on a sharp lower estimate of the energy that relies on relaxation. The new theory is then used to extend existing models for diffusion induced segregation (DIS) in the case of (Zn,Fe)S single crystals. Numerical simulations based on finite elements are carried out and the results are compared with former computations of the homogeneous case.

1 Introduction

The elastic energy of a two-phase solid with microstructure depends in a complicated way on the geometrical distribution of the phases on the microscale. The well-known theory by Eshelby, [1], assumes a linear stress-strain relationship and thus yields apparantly unreasonable predictions for inhomogeneous materials. In this article we take up recent ideas in [2] on the relaxation of a two-well energy that will improve the validity and applicability of the mechanical theory.

The derived results are quite general and have direct applications to crystallography. The mathematical model uses a multiscale approach and describes the elastic behaviour of the material on three different length scales as illustrated in Fig. 1. On the smallest length scale, covering the range of 10nm-50nm, microstructure is dominating. This length scale is usually not taken into account in standard diffusion models. The second length scale is a mesoscopic length scale and averages over the microscale. In the formal description, this corresponds to a relaxation of the microscopic energy using the translation method, see [3] for an introduction, but the philosophy will be explained later in this article. Finally, the macroscopic length scale is in the range of several hundred μm and is the typical length scale considered in simple diffusion models where the material is locally homogeneous. Mathematically, the passage from the mesoscale to the macroscopic length scale is modelled by the convexification (homogenisation) of the mesoscopic energy.
The ansatz presented below has two very appealing aspects. First, an explicit formula for the nonlinear elastic energy on the macroscale is obtained that only depends on macroscopic properties of the material. Therefore in the final implementation, the technical steps of the mathematical derivation need not be considered any more and it is enough to solve the macroscopic equations with the new nonlinear elastic energy and the new continuity equation. The smaller length scales need not be resolved numerically thereby tremendously reducing

[*] Corresponding author: e-mail blesgen@mis.mpg.de, Phone: +049 341 9959 804, Fax: +049 341 9959 658

the computational costs. Secondly, the derived theory is complete, i.e. it correctly describes the properties of the material with ANY order of lamination, provided the material is free of impurities.

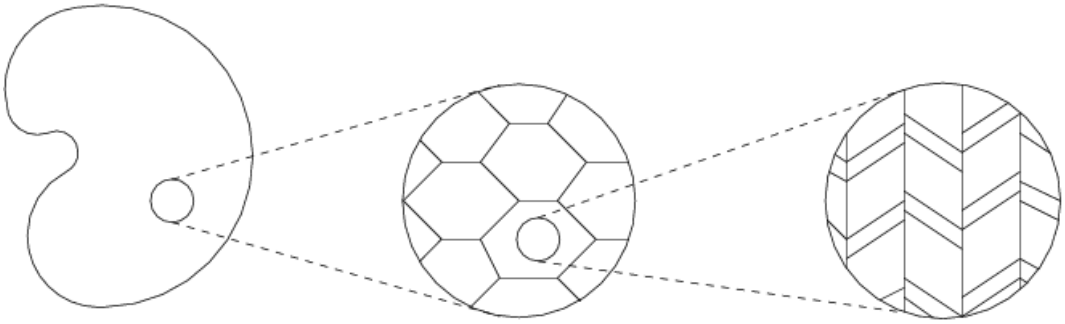

Fig. 1 Schematic plot of the macroscopic, mesoscopic and microscopic length scales of a crystal.

Historically, the theoretical treatment of the outlined multiscale-elasticity problem is quite young. It was first addressed in [4]. In [5], explicit constructions of microstructures were carried out and the lower bound was computed using Fourier analysis, a method which is no longer applicable if the elastic tensors are different. In [6] for the first time arbitrary elastic moduli were considered, but still equal transformation strains were assumed. In this article, we are going to study a general two-dimensional structure without imposing any spurious assumptions. There are only very few restrictions to the derived theoretical model which are discussed in the last section. Former difficulties in 3D, see the discussions in [7] and [8], are overcome by the ansatz.

In the second part of this article we shall apply the new theory to model diffusion induced segregation (DIS) on (Zn,Fe)S single crystals taking the microstructure into account, thereby continuing the earlier studies [9-12] on these systems, where the so-called chalcopyrite disease within sphalerite is studied. Therein the reaction models concerning atomistic mechanisms implying vacancy and metal diffusion as well as redox conditions from experimental DIS were used for the simulations. The corresponding experimental studies simulating natural DIS showed that primary sphalerites bearing Fe > 3 at. % can be provoced to show DIS of Cu-Fe-S-phases, if firstly Fe^{2+} is oxidized to Fe^{3+} by increasing sulfur fugacity. If then Cu diffuses into these sphalerites, Cu reacts with Fe^{3+} to form e.g. chalcopyrite (ccp), i.s.s. (intermediate solid solution within the Cu-Fe-S-system). The natural phenomena and experimental results for i.s.s.-respectively DIS-ccp are exemplary shown in Figure 2.

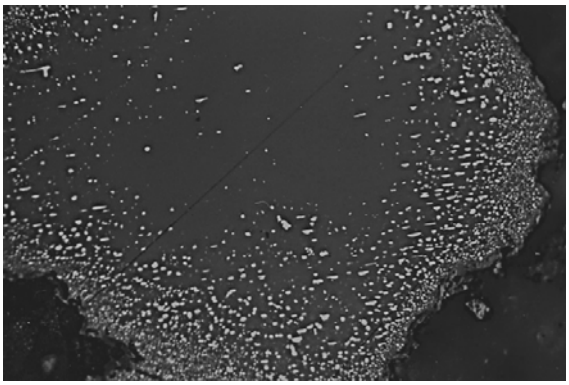

Fig. 2 Fe-bearing sphalerite crystal (grey) with DIS-ccp (light) from mineralized hydrothermal veins of East Banke, Nigeria. At the rim of the crystal the DIS-particles are fine-grained, whereas towards to the core the segregation particles become larger due to coarsening. Width of LM-micrograph 420μm, reflected light, 1. Polar., oil.

This article is organized in the following way. In Section 2 the multiscale theory for elasticity is derived. In Section 3 some numerical simulations are done. We end with a short discussion of the presented results and an outlook in Section 4.

2 Determination of the elastic energy in the presence of microstructure

Let Ω be the reference configuration of the crystal. We denote by

$$\Phi(t):\Omega\to R^D \text{ for } t>0$$

the time-dependent deformation of the crystal. In particular, Φ is sufficiently smooth and invertible with $\det(\nabla\Phi)>0$. We assume that the deformations are small, such that the displacement u is given by

$$\Phi(t)=\mathrm{Id}+u(t).$$

With the help of u the (linearised) local strain tensor can be written as

$$\varepsilon(u)=\tfrac{1}{2}(\nabla u+\nabla u^t), \text{ or equivalently } \varepsilon_{ij}(u)=\tfrac{1}{2}(\partial_i u_j+\partial_j u_i).$$

We apply Landau theory and introduce the macroscopic phase parameter $\chi\in[0,1]$. For $\chi(x,t)=1$ chalcopyrite is present at time t in space point $x\in\Omega$, for $\chi(x,t)=0$ sphalerite is present and for $\chi(x,t)=0.5$, both phases are equally developed. For the elastic energy of the k-th phase we set

$$W_k(\varepsilon):=\tfrac{1}{2}(C_k(\varepsilon-\varepsilon_k^e)):(\varepsilon-\varepsilon_k^e),$$

where C_k is the positive definite second-order elasticity tensor (in Voigt notation, [13]) and ε_k^e is the eigenstrain of the k-th phase. By the above setting, the elastic energy W_k within each laminate agrees with Eshelby's theory.

We assume that the optimal displacement is attained on a time scale much faster than the time scale significant for diffusion such that the energy is minimal among all allowed microscopic configurations with preset phase volume and prescribed boundary conditions, i.e.

$$\overline{W}(\overline{\chi},\overline{\varepsilon})(y)=\inf_{<\chi>=\overline{\chi}}\ \inf_{u|\partial B=\overline{\varepsilon}\cdot x}\ \tfrac{1}{|B|}\int_B \chi(x)W_1(\varepsilon(u(x)))+(1-\chi(x))W_2(\varepsilon(u(x)))dx. \quad (1)$$

To distinguish between the different length scales, we mark here and below all macroscopic variables by a bar. In particular, $\overline{\chi}=<\chi>:=\tfrac{1}{|B|}\int_B\chi(x)dx$ is the average of χ in a ball B around y and $\overline{\varepsilon}$ is the macroscopic strain. The value of $\overline{W}$ is the macroscopic average of microscopic properties within the ball B and can be shown not to depend on the radius of B.

In the following we try to keep the presentation of mathematics as short as possible. We do not repeat the proof of statements that are well established in the aforementioned mathematical references. Subsequently we present and explain the five key steps to explicitly compute the nonlinear elastic energy $\overline{W}$.

Step 1: Convexification of the elastic energy
We remind that a quasiconvex function φ fulfills

$$\varphi(\overline{\varepsilon})\le\inf_{u|\partial B=\overline{\varepsilon}\cdot x}\tfrac{1}{|B|}\int_B\varphi(\varepsilon(u(x)))\,dx \quad (2)$$

for a ball B. In particular, every convex function is quasi-convex. A good reference for background reading on convex analysis is [14], where also the notion of rank-I convexity is explained.

In D space dimensions, let S specify the set of symmetric DxD matrices with real coefficients. Then, for $\beta \geq 0$ and every quasiconvex function $\varphi : S \to R$,

$$\overline{W}(\overline{\chi},\overline{\varepsilon}) \geq \max_{\beta\geq 0, W_k-\beta\varphi \text{ convex}} \min_{\varepsilon_1,\varepsilon_2\in S,\, \overline{\chi}\varepsilon_1+(1-\overline{\chi})\varepsilon_2=\overline{\varepsilon}} \{\overline{\chi}(W_1-\beta\varphi)(\varepsilon_1)+(1-\overline{\chi})(W_2-\beta\varphi)(\varepsilon_2)+\beta\varphi(\overline{\varepsilon})\}. \qquad (3)$$

This formula is geometrically clear, stating that $\overline{W}$ can be estimated from below by its convexification. Fig. 3 illustrates the statement and sketches the elastic energy, its convexification, and the minimisers.
[[For a formal proof, we observe that due to property (2),

$$\overline{W}(\overline{\chi},\overline{\varepsilon})(y) \geq \inf_{<\chi>=\overline{\chi}} \inf_{u|\partial B=\overline{\varepsilon}\cdot x} \tfrac{1}{|B|}\int_B \chi(W_1(\varepsilon)-\beta\varphi(\varepsilon))+(1-\chi)(W_2(\varepsilon)-\beta\varphi(\varepsilon))+\beta\varphi(\overline{\varepsilon})dx.$$

Restricting to convex functions $W_k - \beta\varphi$ (which will turn out necessary in Step 5), we obtain

$$\overline{W}(\overline{\chi},\overline{\varepsilon})(y) \geq \max_{W_k-\beta\varphi \text{ convex}} \min_{<\chi>=\overline{\chi}} \inf_{u|\partial B=\overline{\varepsilon}\cdot x} \tfrac{1}{|B|}\int_B \chi(W_1(\varepsilon)-\beta\varphi(\varepsilon))+(1-\chi)(W_2(\varepsilon)-\beta\varphi(\varepsilon))dx+\beta\varphi(\overline{\varepsilon}).$$

With Jensen's inequality this yields (3).]]

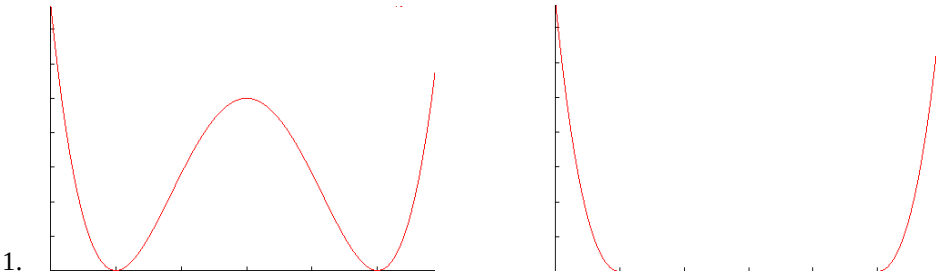

Fig. 3 Elastic energy $\overline{W}$ for fixed $\overline{\varepsilon}$ (left) and its convexification (right). The convexified energy lies below $\overline{W}$ in the originally concave region, and coincides with $\overline{W}$ in the originally convex region of $\overline{W}$.

Step 2: Determination of the convex region and particular choice of φ

As is shown in [15], in 2D the functions $W_k - \beta\varphi$ are convex exactly for $\beta \in [0, \gamma_*]$, where the constant γ_* is computed by $\gamma_* = \min\{\gamma_1, \gamma_2\}$, with γ_k the reciprocal of the largest eigenvalue of the matrix $C_k^{-1/2} Q C_k^{-1/2}$ and Q is given by $Q\begin{pmatrix} \varepsilon_{11} & \varepsilon_{12} \\ \varepsilon_{12} & \varepsilon_{22} \end{pmatrix} = \begin{pmatrix} -\varepsilon_{22} & \varepsilon_{12} \\ \varepsilon_{12} & -\varepsilon_{11} \end{pmatrix}$ in 2D.

To make further progress, it turns out that the appropriate choice in (3) which leads to sharp estimates in 2D is $\varphi(\varepsilon) = -\det(\varepsilon) = \varepsilon_{12}^2 - \varepsilon_{11}\varepsilon_{22}$ which is quasiconvex. We obtain

$$\overline{W}(\overline{\chi},\overline{\varepsilon}) \geq \max_{0\leq\beta\leq\gamma_*} W_{\overline{\chi}}(\beta,\overline{\varepsilon}) \qquad (4)$$

with

$$W_{\overline{\chi}}(\beta,\overline{\varepsilon}) := \min_{\varepsilon_1,\varepsilon_2\in S,\, \overline{\chi}\varepsilon_1+(1-\overline{\chi})\varepsilon_2=\overline{\varepsilon}} \left[\overline{\chi}W_1(\varepsilon_1)+(1-\overline{\chi})W_2(\varepsilon_2)-\beta\overline{\chi}(1-\overline{\chi})\varphi(\varepsilon_2-\varepsilon_1)\right]. \qquad (5)$$

Step 3: Computation of the optimal strains

Since φ is quadratic we can write $\varphi(\varepsilon) = \frac{1}{2}(Q\varepsilon):\varepsilon$, with $Q\varepsilon := \varepsilon - (\varepsilon_{11}+\varepsilon_{22})\mathrm{Id}$ such that $\varphi'(\varepsilon) = Q\varepsilon$. Let $\varepsilon_1^* = \varepsilon_1^*(\beta,\overline{\chi},\overline{\varepsilon})$, $\varepsilon_2^* = \varepsilon_2^*(\beta,\overline{\chi},\overline{\varepsilon})$ be the minimising strains on the right of (5) and let Z denote the argument within brackets […] in (5). Then we find the optimal strains by differentiating Z with respect to ε_1 and ε_2:

$$0=\frac{\partial Z}{\partial \varepsilon_1}(\varepsilon_1^*,\varepsilon_2^*)=\overline{\chi}C_1(\varepsilon_1^*-\varepsilon_1^e)+\beta\overline{\chi}(1-\overline{\chi})Q(\varepsilon_2^*-\varepsilon_1^*),$$
$$0=\frac{\partial Z}{\partial \varepsilon_2}(\varepsilon_1^*,\varepsilon_2^*)=(1-\overline{\chi})C_2(\varepsilon_2^*-\varepsilon_2^e)-\beta\overline{\chi}(1-\overline{\chi})Q(\varepsilon_2^*-\varepsilon_1^*). \quad (6)$$

Cancelling $\overline{\chi}$ in (6a) and $(1-\overline{\chi})$ in (6b), then subtracting (6b) from (6a) yields

$$C_1(\varepsilon_1^*-\varepsilon_1^e)-C_2(\varepsilon_2^*-\varepsilon_2^e)+\beta Q(\varepsilon_2^*-\varepsilon_1^*)=0. \quad (7)$$

Exploiting the condition $\overline{\chi}\varepsilon_1^*+(1-\overline{\chi})\varepsilon_2^*=\bar{\varepsilon}$, the identity (7) can be rewritten as

$$((1-\overline{\chi})C_1+\overline{\chi}C_2-\beta Q)\varepsilon_1^*=(C_2-\beta Q)\bar{\varepsilon}+(1-\overline{\chi})(C_1\varepsilon_1^e-C_2\varepsilon_2^e),$$
$$((1-\overline{\chi})C_1+\overline{\chi}C_2-\beta Q)\varepsilon_2^*=(C_1-\beta Q)\bar{\varepsilon}-\overline{\chi}(C_1\varepsilon_1^e-C_2\varepsilon_2^e).$$

Since $(1-\overline{\chi})C_1+\overline{\chi}C_2-\beta Q=(1-\overline{\chi})(C_1-\beta Q)+\overline{\chi}(C_2-\beta Q)$ is for $0\le\beta\le\gamma_*$ the sum of the two positive definite and thus invertible matrices $(C_1-\beta Q)$ and $(C_2-\beta Q)$, the matrix on the left is also invertible and we find the explicit formulas for the optimal strains

$$\varepsilon_1^*=((1-\overline{\chi})C_1+\overline{\chi}C_2-\beta Q)^{-1}[(C_2-\beta Q)\bar{\varepsilon}+(1-\overline{\chi})(C_1\varepsilon_1^e-C_2\varepsilon_2^e)],$$
$$\varepsilon_2^*=((1-\overline{\chi})C_1+\overline{\chi}C_2-\beta Q)^{-1}[(C_1-\beta Q)\bar{\varepsilon}-\overline{\chi}(C_1\varepsilon_1^e-C_2\varepsilon_2^e)].$$

Step 4: A lower bound on the elastic energy

We have $\overline{W}(\overline{\chi},\bar{\varepsilon})\ge\breve{W}(\overline{\chi},\bar{\varepsilon})$, where

$$\breve{W}(\overline{\chi},\bar{\varepsilon}):=\overline{\chi}W_1(\varepsilon_1^*)+(1-\overline{\chi})W_2(\varepsilon_2^*)-\beta^*\overline{\chi}(1-\overline{\chi})\varphi(\varepsilon_2^*-\varepsilon_1^*),$$

and β^* is the unique solution of $\det((\varepsilon_2^*-\varepsilon_1^*)(\beta,\varepsilon))=0$. To justify this estimate, from the definition (5) of W_χ we see that $\beta\mapsto W_\chi(\beta,\bar{\varepsilon})$ is either constant or strictly concave. If it is constant, then $\varepsilon_2^*-\varepsilon_1^*=0$ which because of (7) is only possible if $C_2(\bar{\varepsilon}-\varepsilon_2^e)=C_1(\bar{\varepsilon}-\varepsilon_1^e)$. But then, $\overline{W}(\overline{\chi},\bar{\varepsilon})=\breve{W}(\overline{\chi},\bar{\varepsilon})$. In the other case that $\beta\mapsto W_\chi(\beta,\varepsilon)$ is strictly concave, the maximum is at $\beta=0$ when $\varphi((\varepsilon_2^*-\varepsilon_1^*)(0,\bar{\varepsilon}))\ge 0$ and at $\beta=\gamma_*$ if $\varphi((\varepsilon_2^*-\varepsilon_1^*)(0,\bar{\varepsilon}))<0$. In both cases, β_* is unique with $\varphi((\varepsilon_2^*-\varepsilon_1^*)(\beta_*,\bar{\varepsilon}))=0$ and $\overline{W}(\overline{\chi},\bar{\varepsilon})\ge\breve{W}(\overline{\chi},\bar{\varepsilon})$.

These considerations can be subsumed in the explicit representation

$$\breve{W}(\overline{\chi},\bar{\varepsilon})=\begin{cases} W_\chi(0,\bar{\varepsilon}), \text{ if } C_2(\bar{\varepsilon}-\varepsilon_2^e)=C_1(\bar{\varepsilon}-\varepsilon_1^e), & \text{(Regime 0)}\\ W_\chi(0,\bar{\varepsilon}), \text{ if } \varphi(\varepsilon_2^*(0,\bar{\varepsilon})-\varepsilon_1^*(0,\bar{\varepsilon}))>0, & \text{(Regime 1)}\\ W_\chi(\gamma_*,\bar{\varepsilon}), \text{ if } \varphi(\varepsilon_2^*(\gamma_*,\bar{\varepsilon})-\varepsilon_1^*(\gamma_*,\bar{\varepsilon}))<0, & \text{(Regime 3)}\\ W_\chi(\beta_*,\bar{\varepsilon}), \text{ otherwise.} & \text{(Regime 2)}\end{cases} \quad (8)$$

The four regimes in (8) have the following crystallographic interpretation. Laminates of rank-I and rank-II are sketched in Fig. 4 and Fig. 5.

Regime 0: The material is homogeneous and the energy does not depend on the microstructure.
Regime 1: There exist two optimal rank-I laminates.
Regime 2: The unique extremal microstructure is a rank-I laminate.
Regime 3: There exist two optimal rank-II laminates.

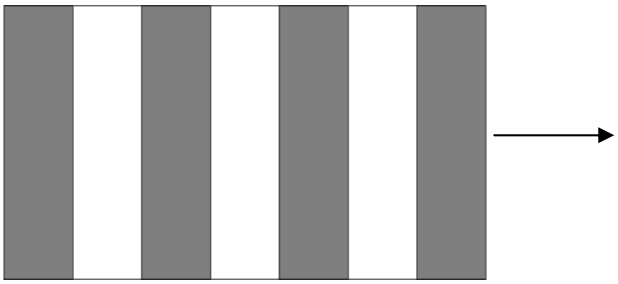

Fig. 4 A two-phase rank-I laminate in two space dimensions with corresponding normal vector. The strains are constant in the shaded and in the unshaded regions. The volume fraction of both phases, 0.5 in the picture, is prescribed by the macroscopic parameter $\overline{\chi}$.

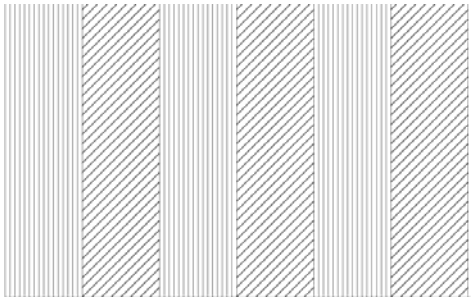

Fig. 5 A two-phase rank-II laminate in two space dimensions. The widths h_1 and h_2 of the slabs should be much larger than the thickness of the layers between each slab.

Step 5: Upper bound on the elastic energy and construction of extremal microstructures
The definition of $\overline{W}$ in (1) immediately implies

$$\overline{W}(\overline{\chi},\overline{\varepsilon})(y) \leq \inf_{u|\partial B=\overline{\varepsilon}\cdot y} \frac{1}{|B|}\int_B \chi(x)W_1(\varepsilon(u(x))) + (1-\chi(x))W_2(\varepsilon(u(x)))\,dx =: \widehat{W}(\overline{\varepsilon},\overline{\chi}),$$

where χ under the integral may represent any microstructure with $<\chi>=\overline{\chi}$. So we have

$$\breve{W}(\overline{\chi},\overline{\varepsilon}) \leq \overline{W}(\overline{\chi},\overline{\varepsilon}) \leq \widehat{W}(\overline{\varepsilon},\overline{\chi}).$$

The established estimates are so sharp that it is possible to find a microstructure χ for which the upper and lower bound coincide in each of the four regimes,

$$\breve{W}(\overline{\chi},\overline{\varepsilon}) = \widehat{W}_{\chi}(\overline{\varepsilon}) = \overline{W}(\overline{\chi},\overline{\varepsilon}), \tag{9}$$

and to verify that the microstructure in the above classification is optimal. This construction can be carried out in the spirit of [5] and we do not present it here. As a result of this construction, the formal characterization of the four regimes stated above follows.

As a consequence to (9) we see in particular that (8) supplies us with an explicit definition of the multiscale elastic energy $\overline{W}$ in the presence of microstructure. This explicit formula (8) is the basis of the numerical studies in the subsequent section.

3 Numerical Simulations

Now we present the results of a numerical simulation with high resolution that illustrates the effects of the non-linear elastic energy. The finite element triangulation of Ω as well as the time step Δt are not optimized

during the computations. The simulations are carried out for a two-dimensional layer Ω and (10)-(13) below are solved in dimensional form. For the physical parameters the measured quantities are used. The diffusivities are taken from the measured data in [16]. For the dependence of D_{CU} on the Fe and Zn concentration the results of molecular dynamics computations in [17] are reused. The article [17] contains as well the approximate calculation of the elastic constants of chalcopyrite by quantum mechanical computations, as these parameters cannot yet be measured experimentally.

The numerical implementation makes use of linear finite elements and a very efficient Quasi-Newton method that relies on GMRES to solve the linearized equations, see [9] for an introduction of the method. We shall compare the simulations of the new enhanced model with the earlier numerical experiments in [18], where a linear elastic energy was studied. In the sequel we shall refer to these simulations as the results of the linear model.

Numerically we compute for $t \geq 0$ the solution $\bar{c}_1, \bar{c}_2, \bar{c}_3, \bar{c}_4, \bar{\chi}, \bar{u}$ such that in $\Omega \subset \mathrm{R}^2$ for $t > 0$

$$0 = \mathrm{div}\Big(d \nabla \frac{\partial f}{\partial c_j}\Big) + k(\bar{c}_2 - \bar{c}_1) - \gamma k \bar{c}_1 \bar{c}_3, \tag{10}$$

$$\partial_t \bar{c}_i = \mathrm{div}(\textstyle\sum_{j=2}^{3} L_{ij} \nabla \frac{\partial f}{\partial \bar{c}_j}(\bar{c}, \bar{\chi})), \ 2 \leq i \leq 3, \tag{11}$$

$$\partial_t \bar{\chi} = \lambda^2 \Delta \bar{\chi} - \psi(c_3, \bar{\chi}, \varepsilon(\bar{u})), \tag{12}$$

$$0 = \mathrm{div}\Big(\partial_\varepsilon \overline{W}(\bar{\chi}, \varepsilon(\bar{u}))\Big). \tag{13}$$

Equation (13) is the common continuity equation for the elastic stress $\partial_\varepsilon \overline{W}(\bar{\chi}, \varepsilon(\bar{u}))$ and follows from Newton's second law under the assumption that the acceleration $\rho \partial_{tt} \bar{u}$ (where ρ is the mass density) which originally appears on the left is negligible. The system (10)-(13) is completed with the initial values $\bar{c}_i(\cdot,0) = \bar{c}_{0i}$, $i = 2,3$, $\bar{\chi}(\cdot,0) = \bar{\chi}_0$ in Ω and the Neumann boundary conditions $\partial_\nu \bar{c}_1 = \partial_\nu \bar{c}_2 = \partial_\nu \bar{\chi} = 0$ and Dirichlet boundary condition $\bar{c}_3 = g_3$ on $\partial\Omega$. In this formulation the functions $\bar{c}_i = \bar{c}_i(x,t)$ trace the concentrations of the involved constituents, where we used the notations

$$\bar{c}_1 \approx \mathrm{Fe}^{3+}, \bar{c}_2 \approx \mathrm{Fe}^{2+}, \bar{c}_3 \approx \mathrm{Cu}^{+}, \bar{c}_4 \approx \mathrm{Zn}^{2+}, \bar{c}_5 \approx \text{vacancies}.$$

As explained in the earlier work we have the relationships $\bar{c}_5 = 0.5\bar{c}_1$, $\bar{c}_4 = 1 - 0.5\bar{c}_1 - \bar{c}_2 - \bar{c}_3$, and the (constant) sulphur concentration $\bar{c}_6 \equiv 0.5$. In agreement with the conditions during the crystallographic experiments the temperature T is constant. This also simplifies the formulation within the framework of non-equilibrium thermodynamics.

The free energy F in (11) is given by

$$F(\bar{c}, \bar{u}, \bar{\chi}) = \int_\Omega f(\bar{c}, \bar{u}, \bar{\chi})\, dx = \int_\Omega \textstyle\sum_{i=1}^{4} \beta_i^l \bar{c}_i \ln \bar{c}_i + \overline{W}(\bar{\chi}, \varepsilon(\bar{u}))\, dx,$$

where $\overline{W}$ is the non-linear elastic energy derived in Formula (8).

The phase transition sphalerite to chalcopyrite is a transition cubic to tetragonal. In three space dimensions, there are three variants how the cubic unit cell can be transformed to a tetragonal unit cell as illustrated in Fig. 6, giving rise to the 3 possible eigenstrains

$$\varepsilon_I^e = \begin{pmatrix} u & 0 & 0 \\ 0 & u & 0 \\ 0 & 0 & v \end{pmatrix}, \varepsilon_{II}^e = \begin{pmatrix} u & 0 & 0 \\ 0 & v & 0 \\ 0 & 0 & u \end{pmatrix}, \varepsilon_{III}^e = \begin{pmatrix} v & 0 & 0 \\ 0 & u & 0 \\ 0 & 0 & u \end{pmatrix}.$$

In this formula, $u := \frac{a_1}{a_0} - 1$, $v := \frac{c_1}{a_0} - 1$, and $a_0 = 5.403\,\text{Å}$ is the lattice parameter of cubic sphalerite, $a_1 = b_1 = 5.286\,\text{Å}$, $c_1 = 10.41\,\text{Å}$ are the lattice parameters of tetragonal chalcopyrite. A general classification of the eigenstrains of all possible lattice geometries can be found in [19].

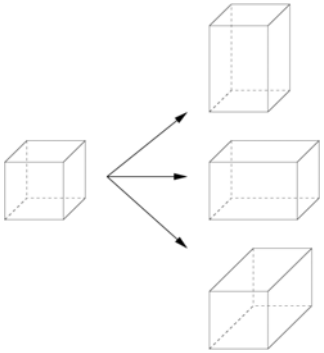

Figure 6 The three geometric variants of a cubic to tetragonal lattice transformation in 3D.

Physical Parameters: $\Omega = 1{,}2 \cdot 10^{-3}\mathrm{m} \times 6 \cdot 10^{-4}\mathrm{m}$, $T = 500°C$, $\varepsilon^2 = 3 \cdot 10^{-9}\mathrm{m}$, $D_{CU} = 2.6 \cdot 10^{-4} m/s$, $D_{Zn} = 1.85 \cdot 10^{-7} m/s$, $D_{Fe} = 1.26 \cdot 10^{-4} m/s$.

Triangulation Data: 131841 points, 131072 triangles, $h = 10^{-8}$.

General Parameters: $\varepsilon_{\mathrm{GMRES}} = 4 \cdot 10^{-5}$, $\Delta t = 4 \cdot 10^{-3}$, $\eta = 10^{-8}$, $\beta = 20$, $\delta = 4$.

Initial conditions: $\bar{c}_{01} \equiv 0.001$, $\bar{c}_{02} = 0.3$, $\bar{c}_{03} = 0.001$ and $\bar{\chi}_0$ is the minimiser of $\bar{\chi} \mapsto F(\bar{c}_0, \bar{\chi})$.

Boundary conditions: $\partial_n \bar{c}_1 = \partial_n \bar{c}_2 = 0$, $\bar{c}_3 = 0.25$ and $\partial_n \bar{\chi} = 0$ on $\partial\Omega$.

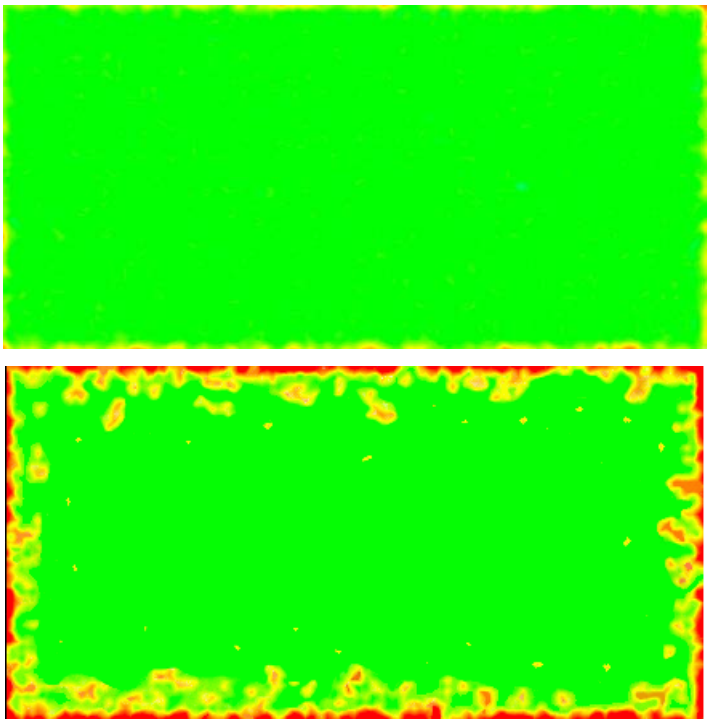

Figure 7 Dense isoline plot of the phase parameter for t=24d (top) and t=125d (bottom). At t=0d only sphalerite (green) is present (not displayed). As copper enters the crystal, chalcopyrite (red) forms close to the crystal boundary. The interfacial regions are rendered yellow. The segregation starts with small islands that arise from nucleation and finally form a connected front.

We do not display the time evolutions of Zn and Cu^+. Both behave as was pointed out in the earlier papers on chalocopyrite disease. Zn moves out of the matrix and is replaced by Cu^+. The concentration of Fe^{3+} + Fe^{2+} is constant and invariant in time and space. So, the global behaviour of the system is similar to the earlier studies.

The shape of the phase transitions is influenced by the elastic energy, leading to preferred directions and stretched interfaces. In first approximation, for locally isolated phases that do not compete with neighbouring phases, this agrees with the earlier numerical simulations based on the linearised elastic energy. As a new effect, the nonlinear elastic energy gives rise to little kinks at the interfacial layer following the steps of the lamination. This is resolved in more detail in Fig. 8.

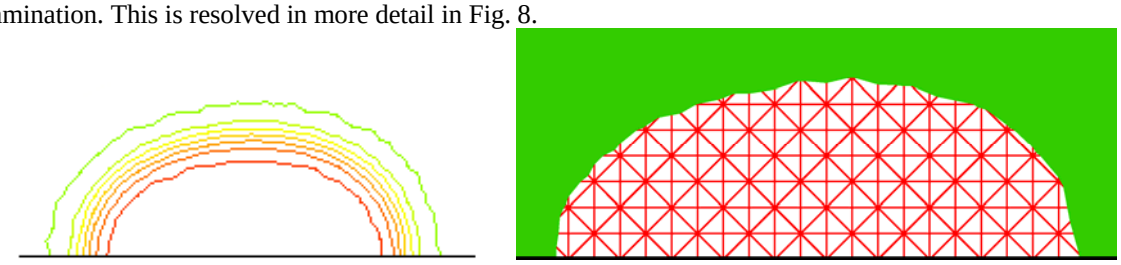

Figure 8 Enlargement of a chalcopyrite phase(red) within sphalerite(green) close to the crystal boundary (solid black line). Left: Plot of the levelsets. Right: Interface and numerical grid. The shape of the chalcopyrite phase is stretched in x-direction similar to the predictions of the linear elasticity model. In the absence of elastic energy, the shape of the chalcopyrite phase would be unstretched and form a perfect half-circle. The left and the right picture both reveal little steps of the interface on the scale of the numerical grid.

The situation complicates when two or more adjacent phases interact. The nonlinear elastic energy is far-reaching and has a strong effect on the shape of closeby interfaces. For the microstructural nonlinear elasticity, the phase patterns may locally reveal a dynamical behaviour very different from the linear case. Fig. 9 shows an example of two chalcopyrite phases close to the crystal boundary that alternatingly join, split up and even touch in one point.

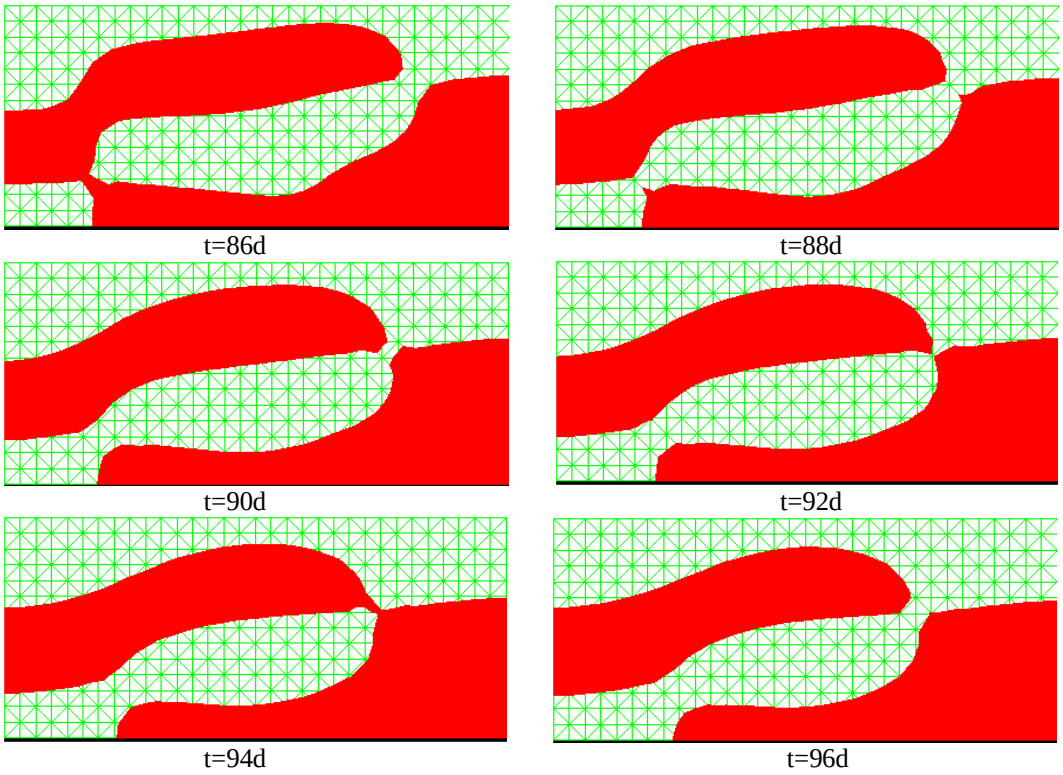

Figure 9 Enlarged bottom section of the crystal (boundary appears as solid black line). Shown is the complicated interaction of two chalcopyrite phases. Alternatingly, the phases melt and split up. At t=88d, each of the chalcopyrite phases has formed a small kink in the direction of its neighbouring phase. At t=92d, the two chalcopyrite phases and the two sphalerite phases touch in one point.

The situation displayed in Fig. 9 can be observed frequently during the computations. The formation of little kinks pointing to a neighbouring phase as well as the repeated local union and splitting up of neighbouring phases seems to be a typical feature.

4 Discussion of the results and outlook

In this article, a general physical theory for the stored mechanical energy of two-phase elastically stressed solids was derived, taking the microstructural lamination into account. For the basic application of the enhanced nonlinear theory only the elastic constants and the space groups of the pure phases need to be known. From a practical viewpoint, the heavy mathematics of Section 2 can be bypassed and treated as a black box. The presented method is very general and can be readilly transferred to a large class of situations in mineralogy and solid state physics. This makes the ansatz interesting for many applications. Without the explicit formula (8), numerical computations that resolve the microstructure require supercomputer facilities.

The computations of Section 3 showed the similarities to, but also the limits of the standard linear elasticity theory. In conclusion, the studies show that the linear elasticity model gives good predictions of single, isolated phases, but fails to correctly predict the complex, far-ranging interactions of the correct micro-structural model. Especially the intrinsic behaviour illustrated in Fig. 9 is beyond the traditional linear elasticity model.

A qualitative comparison of the predicted numerical segregation speeds of the established linear and the new nonlinear model reveals that in the latter case the segregation occurs somewhat faster, the figures indicate an acceleration by about 2%. Possibly, this is caused by the stronger interaction of the nonlinear energy that results in a quicker arrangement of the phases.
As one main result of [2], it is sufficient to restrict to laminates of order two in two space dimensions and to laminates of order three in three space dimensions. Lamination models of higher order, replacing formula (8), will thus not improve the results stated here. In this regard the developed theory is optimal.

Finally, the following comments on the limitations of the theory deserve attention.

- The presented model is valid for single crystals only. The averaging of $\overline{W}$ fails for polycrystals and it is currently an open question how to proceed in this case. The available theory for polycrystals is quite old; the main references are [20,21].
- For the elastic energy on the microscale a linear stress-strain relationship is assumed. This is once more a simplification that ignores long-range elastic interactions. Additionally, impurities and lattice defects are not incorporated in the theory, but are expected to locally influence the microstructure in the crystal. To correctly capture this, measurements of the in-situ crystallography in experiments are inevitable.
- Explicit formulas of the elastic energy were obtained in two space dimensions by choosing $\varphi = -\det(\varepsilon)$. In 3D one has to choose $\varphi_j(\varepsilon) = f_j(M^t \varepsilon M)$, where M is a symmetric 3x3 matrix and f_j are the diagonal subdeterminants (also called 'minors'), thus $\varphi_1 = \varepsilon_{23}^2 - \varepsilon_{22}\varepsilon_{33}$, $\varphi_2 = \varepsilon_{31}^2 - \varepsilon_{33}\varepsilon_{11}$, $\varphi_3 = \varepsilon_{12}^2 - \varepsilon_{11}\varepsilon_{22}$. Determining the amount of translation γ_*, i.e. characterising the permitted convex sets in 3D, is possible following the arguments in [2]. This is even possible for non-isotropic media.
- In the derivation of formula (8), the independence of the diffusion processes and of the minimization of the elastic energy is tacitly assumed. This assumption of independence is based on the very different time scales of diffusion and elastic response of the material and holds only in approximation.

Acknowledgements This work evolved from a project funded by the Deutsche Forschungsgemeinschaft under Lu 312/6-3 within the "Schwerpunktprogramm: Strukturgradienten". The author thanks Prof. Dr. K. Bente for valuable discussions.

References

[1] J.D. Eshelby, Proceed. Royal Soc. London Series A-Math. Physical and Engineering Sciences, **241**, 376 (1957).
[2] I.V. Chenchiah and K. Bhattacharya, Arch. Rat. Mech. Anal. **187**, 409 (2008).
[3] A.V. Cherkaev, Variational Methods for structural optimization, Applied Math. Sciences v. 140 (Springer, New York, 2000).
[4] L.V. Gibiansky, and A.V. Cherkaev, Design of composite plates of extremal rigidity, Tech. Report 914 (Ioffe Techn. Institute, Leningrad, USSR, 1984).
[5] R.V. Kohn, Cont. Mech. Thermodyn. **3**, 193 (1991).
[6] Y. Grabovsky, Proceed. Royal Soc. London. Series A-Math. Physical and Engineering Sciences **452**, 919 (1996).
[7] S. Govindjee, A. Mielke, and G.J. Hall, Journ. Mech. Phys. Solids **51**, 1 (2003).
[8] H.J. Jou, P.H. Leo, and J.S. Lowengrub, Journ. Comp. Phys. **131**, 109 (1997).
[9] T. Blesgen, S. Luckhaus, and K. Bente, Cryst. Res. Technol. **3**7, 570 (2002).
[10] T. Blesgen, S. Luckhaus, and K. Bente, Cryst. Res. Technol. **39**, 969 (2004).
[11] K. Bente, and T. Doering, Eur. J. Mineral. **10**, 465 (1993).
[12] K. Bente, and T. Doering, Min. Petrol. **53**, 285 (1995).
[13] J.F. Nye, Physical Properties of Crystals: their representation by tensors and matrices (Clarendon Press, Oxford, 1964).
[14] I. Ekeland, and R. Temam, Convex Analysis and variational problems (North-Holland, Amsterdam, 1976).
[15] K. Bhattacharya, Cont. Mech. Thermodyn. **5**, 205 (1993).
[16] P. Nelkowski, and S. Bollmann, Min. Petrol. **27**, 1302 (1969).
[17] T. Blesgen, London Mathematical Society, Modell. Simul. Mat. Sci. Eng. **14**, 389 (2006).
[18] T. Blesgen, Cryst. Res. Technol. **3**7, 969 (2002).
[19] K. Bhattacharya, and R. V. Kohn, Arch. Rat. Mech. Anal. **139**, 99 (1997).
[20] G. Sachs, Z. Ver. Dt. Ing. **72**, 734 (1928).
[21] G.I. Taylor, J. Inst. Metals **62**, 307 (1938).